High Temperature Behavior during Solidification of Peritectic Steels under Continuous Casting Conditions

Robert Pierer, Christian Bernhard

Christian Doppler Laboratory of Metallurgical Fundamentals of Continuous Casting Processes;
University of Leoben; Franz Josef Str. 15; 8700 Leoben; Austria

Keywords: High Temperature Behavior, Contraction Force, Depression Formation

Abstract

The high temperature behavior of solidifying steel is of great importance for the continuous casting process. In the process, the shrinkage of the solidifying steel plays an important role, because it affects the surface and internal quality of the cast product. The calculation of shrinkage using mathematical models is strongly influenced by the material data and the constitutive equations, which are not very well known at temperatures close to the solidus.

The influence of the carbon content on the solidification and shrinkage is investigated using a modified hot tensile test, which allows the measurement of the contraction force during solidification. In addition, a thermo-mechanical model of the test is developed, based on an elasto-plastic approach and considering hardening and softening mechanisms due to the high temperature deformation process.

The modeling results are in excellent agreement with the experimental results and provide a better understanding of the phenomena occurring during the shrinkage of steel.

Introduction

One important part of numerical modeling of the continuous casting process represents the initial solidification in the mold in conjunction with heat flow, mechanical behavior of the solidifying steel shell, thermal distortion of the mold, oscillation mark formation and initial shell strength. Steel shrinkage (in the liquid phase) and thermal contraction (in the solid phase) together with the mechanical behavior of the solidifying steel shell have a major influence on crack formation (surface cracks as well as hot tear cracks) and other defects appearing during continuous casting. From many studies on this topic - summarized in a comprehensive study by Wolf [1] - it was pointed out that steel grades with a carbon content between 0.1 and 0.12 wt-% are more sensitive to crack formation and more difficult to cast than others. This behavior is explained by a minimum of heat flux in the mold due to uneven meniscus shell growth. However, the calculation of shrinkage and thermal contraction is a complicated task and the results are strongly influenced by the material data and the material constitutive equations, which are not very well known at temperatures close to the solidus temperature T_S.

The present paper presents a test method for the measurement of contraction behavior (contraction force) during initial solidification. The experimentally determined results of a test series with different carbon contents (0.05 wt-% - 0.2 wt-%) are illustrated. Furthermore, a mathematic model was developed

in order to describe the thermo-mechanical behavior during the experiment. The model is based on a simple geometry of the solidified cross-section. An elasto-plastic approach is used, which in addition considers hardening and softening mechanisms of high temperature deformation. Both the results of the experiment and the results of the calculations are presented and discussed. Finally, the calculation results are applied on a model of depression formation in order to illustrate the influence of the contraction force on the uneven shell growth.

Experiment

The SSCT-test (Submerged Split Chill Tensile) is a proven in-situ tensile test method, with conditions very similar to those in the continuous casting process. The experiment has been developed over more than ten years in order to determine the high-temperature mechanical properties and crack susceptibility of steel [2-4]. A solid steel test body, split in two halves, is submerged into the liquid melt in an induction furnace. The surface of the test body is spray-coated with a thin zirconium oxide layer. The coating controls the cooling conditions and minimizes friction. A steel shell solidifies around the test body with the main crystallographic orientation perpendicular to the interface, similar to the situation in a continuous casting mould. The force between the upper and lower part of the test dummy is measured by a load cell, the position of the lower part by an inductive position sensor. A servo-hydraulic controller controls force and position. This allows a number of different testing procedures:

Hot tensile test (SSCT-test): after a certain holding time, the lower half of the test body is moved downwards at a controlled velocity at strain rates typically between 10^{-3} and 10^{-2} s^{-1}. The necessary tensile force is recorded.

Contraction test: after initial solidification the shell is pre-loaded with a marginal load. The lower part moves upwards under the contraction force of the solidifying shell, while the resulting displacement Δl is measured.

Contraction force test: the lower part of the test body remains in its original position ($\Delta l=0$), the resulting force (F_C), proportional to the contraction force, is recorded.

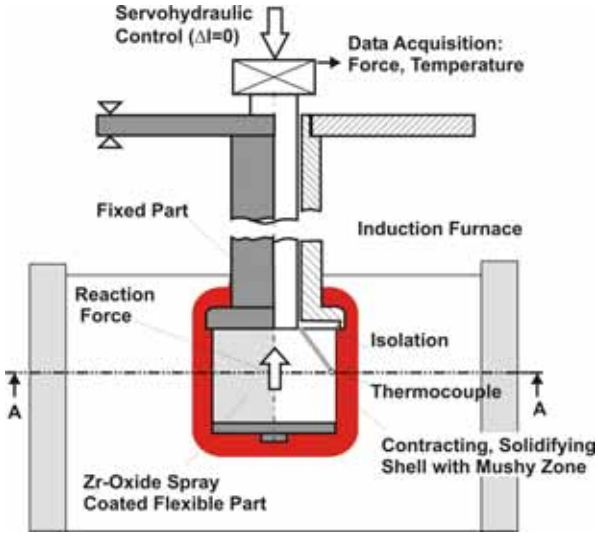

Figure 1: Schematic diagram showing the test method

Figure 1 shows a schematic view of the contraction and the contraction force test method, whereby the geometry of the test body is modified in contrast to the test body of the hot tensile test. This modification allows the investigation of the contraction behavior of solidifying steel, either by measuring the resulting displacement Δl (contraction test), or the force F_C (contraction force test).

Table I. Chemical Composition of Tested Steel Grades

	Steel No.	C	Si	Mn	P	S	Ni	C_p
A	1	0.05	0.29	1.52	0.012	0.004	0.017	0.07
	2	0.07	0.27	1.51	0.012	0.004	0.017	0.09
B	3	0.09	0.29	1.55	0.011	0.008	0.026	0.12
	4	0.13	0.31	1.57	0.014	0.004	0.017	0.15
C	5	0.15	0.28	1.56	0.014	0.005	0.018	0.17
	6	0.20	0.27	1.75	0.014	0.005	0.020	0.23

The present work refers to a contraction force test series with constant cooling conditions, varying the carbon content between 0.05 and 0.20 wt-%. In order to consider the influence of the alloying elements on the peritectic reaction, it is reasonable to use the equivalent carbon content c_p. In the following, all results and their interpretation refer to c_p according to Howe [5]:

$$c_p = [\%C] + 0.04 \cdot [\%Mn] + 0.1 \cdot [\%Ni] - 0.14 \cdot [\%Si] \qquad (1)$$

Table I shows the chemical composition of the tested steel grades, which in addition are classified into type A ($c_p < 0.1\%$), steel B ($0.1\% < c_p < 0.16\%$) and type C ($0.16\% < c_p < 0.51\%$) steel grades. Hence, the solidification behavior of these three steel types can be characterized as follows: the onset of the δ–γ transformation of the type A steels takes place below T_S, whereas the onset of δ–γ transformation of type B steels take place already during solidification. The total range of the δ–γ transformation at the type C steels is above T_S, which means that the transformation is already finished in the mushy zone.

Thermo-Mechanical Modeling of the Contraction Force Test

In order to calculate the resulting contraction force F_C of the experiment a thermo-mechanical model was developed. The thermal analysis is based on the well known heat-conduction equation, which solves the transient energy balance:

$$\rho(T)\frac{\partial H(T)}{\partial t} = \frac{1}{r} \cdot \frac{\partial}{\partial r}\left(r \cdot \kappa(T)\frac{\partial T}{\partial r} \right) \qquad (2)$$

In equation (2) H is the enthalpy, ρ the density, κ the thermal conductivity of steel as a function of temperature T, r and t denote the radius and the time, respectively.

The mechanical analysis is based on a simple geometry of the solidified cross-section, which was first developed for the hot tensile test (SSCT-test) and is described in detail elsewhere [6, 7]. First

calculations [6] were carried out using an elastoplastic approach as follows, where the total strain ε_{tot} of the solidified steel shell is the sum of the elastic strain ε_{el} and the plastic strain ε_{pl}:

$$\varepsilon_{tot} = \varepsilon_{el} + \varepsilon_{pl} \qquad (3)$$

However, elastoplastic models do not account for the influence of different strain rates. Therefore, elasto-viscoplastic models were utilized to consider the strain rate dependence of plastic deformation. Recently, the authors investigated common strain rate dependent constitutive equations using an elasto-viscoplastic approach [7]:

$$\dot{\varepsilon}_{tot} = \dot{\varepsilon}_{el} + \dot{\varepsilon}_{pl} \qquad (4)$$

In equation (4), the total strain rate $\dot{\varepsilon}_{tot}$ is split into the elastic strain rate $\dot{\varepsilon}_{el}$ and the inelastic strain rate $\dot{\varepsilon}_{pl}$. In the mathematic formulation of the hot tensile test the thermal strain ε_{th} is neglected. In the modeling of the contraction force test, as a matter of course, the thermal strain, which acts as the driving force of the experiment, has to be considered. Due to the easier handling and implementation of an elasto-plastic model, the thermo-mechanical description of the contraction force test is based on a rate-independent approach. Regarding the condition of the experiment the sum of the thermal strain, the elastic strain and the plastic strain must be equal to zero:

$$\varepsilon_{th} + \varepsilon_{el} + \varepsilon_{pl} = 0 \qquad (5)$$

The different components of the strain in equation (4) are defined as a function of time, temperature and Fe-phase (δ-Fe and γ-Fe) and are summarized in Table II. The density for δ-Fe and γ-F is calculated according to Harste [8] and for the liquid state as proposed by Jimbo and Cramb [9]. The Young's modulus is also determined for the two Fe-phases [8]. The plastic strain can be computed using the Hollomon stress-strain relationship, assuming nonlinear isotropic hardening ($n \neq 1$). K_P is defined by a simple power law equation to account for thermal activation of the high temperature plasticity, where the constants C and m are assumed as fitting parameters. The strain hardening exponent n is determined following the procedure outlined by Uehara et al. [10]. In this method, Z is calculated applying an assumed average strain rate of $1 \cdot 10^{-4}$ s^{-1}, the corresponding temperature T and the activation energy of deformation according to Harste et al. [11, 12].

Using the Hollomon relationship for the plastic strain in equation (5) results in a description of the problem considering only the hardening process. However, during high temperature deformation it is well known that in addition to the hardening process softening mechanisms occur. In the contraction force test the reaction force is generated due to the fact that thermal contraction is avoided by controlling the elongation ($\Delta l = 0$). It is worth noting that these condition are very similar to the relaxation process. Ilschner [13] formulated the fundamental equation of stress relaxation as follows:

$$\frac{d\sigma}{dt} = -\dot{\varepsilon}_R \cdot E(T) \qquad (6)$$

Equation (6) describes the decrement of stress $\Delta\sigma$ as a function of the plastic relaxation rate $\dot{\varepsilon}_R$ and the Young's modulus E. Such an approach was for example applied by Verdier et al. [14] Smith et al. [15] to describe the static recovery process.

Table II. Relationships Used in Equation (4)

Thermal Strain	$\varepsilon_{th}(T) = \sqrt[3]{\frac{\rho(T_0)}{\rho(T)}} - 1$
Density, ρ[kg/m^3]	$\rho^{\delta} = (8010.71 - 0.4724 \cdot T) \cdot \left(1 + \frac{\%C}{100 - \%C}\right) \cdot (1 + 13.43 \cdot 10^{-3} \cdot \%C)^{-3}$
	$\rho^{\gamma} = (8105.91 - 0.5091 \cdot T) \cdot \left(1 + \frac{\%C}{100 - \%C}\right) \cdot (1 + 8.317 \cdot 10^{-3} \cdot \%C)^{-3}$
	$\rho^{L} = 7100 - 73 \cdot \%C - (0.8 - 0.09 \cdot \%C) \cdot (T - 1550)$
Elastic Strain	$\varepsilon_{el}(T) = \frac{\sigma}{E(T)}$
Young's Modulus, E[MPa]	$E^{\delta} = 208060 \cdot (0.925 - 4.98 \cdot 10^{-4} \cdot T[^{\circ}C])$
	$E^{\gamma} = 208060 \cdot (0.981 - 4.76 \cdot 10^{-4} \cdot T[^{\circ}C])$
Plastic Strain	$\varepsilon_{pl}(T) = \left(\frac{\sigma}{K_P(T)}\right)^{1/n}$
Plastic Resistance, K_P[MPa]	$K_P = C \cdot T^m$
Material Parameter, C [MPa^{-n}K^{-m}]	$C^{\delta} = 2.3208 \cdot 10^{15}$, $C^{\gamma} = 7.6886 \cdot 10^{25}$
Material Parameter, m[-]	$m^{\delta} = -4.7906$, $m^{\gamma} = -7.7847$
Strain Hardening Exponent, n [-]	$n = a \cdot (\ln Z)^4 + b \cdot (\ln Z)^3 + c \cdot (\ln Z)^2 + d \cdot (\ln Z) + e$
	$a = 2.9645 \cdot 10^{-5}$, $b = -1.7141 \cdot 10^{-3}$, $c = 3.4788 \cdot 10^{-2}$, $d = -0.2702$, $e = 0.7140$
Zener-Hollomon Parameter, Z [s^{-1}]	$Z = \dot{\varepsilon} \cdot \exp\left(\frac{Q_{def}}{R \cdot T}\right)$
Activation Energy of Deformation, Q [kJ/mol]	$Q^{\delta} = 240000$, $Q^{\gamma} = 270000$

In the calculation procedure of the contraction force it is assumed that the solidified steel shell is able to develop contraction forces at temperatures below the zero strength temperature (ZST). It should be noted that the contraction force test is a gradient test under unsteady conditions. The temperature inside the steel shell increases nearly linearly from the surface temperature T_{surf} at the interface of the test body and the steel shell up to the liquidus temperature T_L and changes with solidification time. Finally, the stress calculated using equation (5) is reduced by the decrement of stress resulting from equation (6), whereas the plastic relaxation rate is adjusted to get the best agreement with the measured contraction force.

Results and Discussion

The following section is divided into three parts: firstly the experimentally determined results will be discussed, secondly the results of the thermo-mechanical model of the experiment are illustrated and lastly the importance of the contraction force with respect to the formation of depressions (uneven shell growth in the mold) will be demonstrated.

Experimental Results

A detailed review of the results was recently published by Bernhard [16, 17] with the main focus on crack formation. The results of the experiment – the measured contraction force as a function of time – are illustrated in Figure 2.

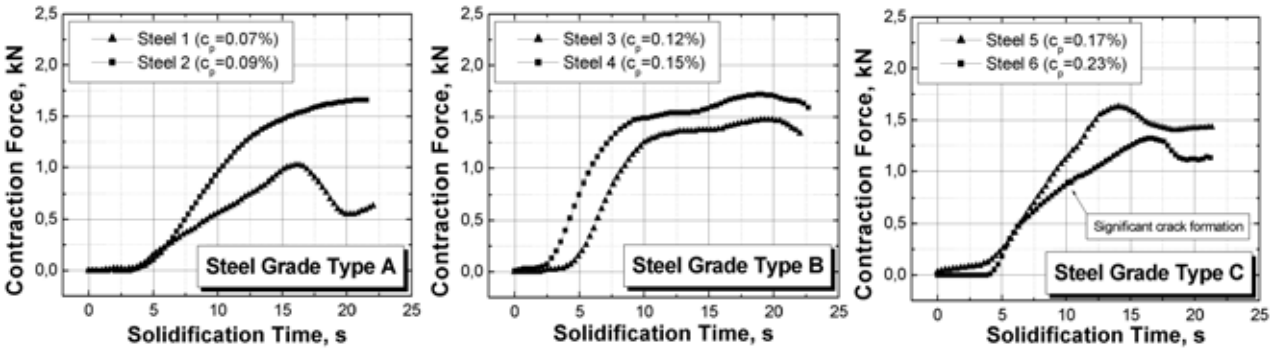

Figure 2: Experimentally determined contraction force as a function of solidification time for three different steel grades

As the above results show, steel 2 is clearly different compared to the other steels. After achieving a maximum value of F_C a decrease in force takes place. In addition the slope of the measured curve is lower compared to the steels with higher carbon content. The characteristic of steel 6 seems to be similar to the curve of steel 1. However, compared to the other steel grades, a significant crack formation was determined, which explains the measured characteristic. Generally, the steel grades type C show the highest susceptibility to cracking. Investigations of the crack formation of steel 1 indicate the lowest numbers of cracks. Therefore, crack formation cannot be the reason for the measured characteristic of steel 1. The characteristics of steel 2 with an equivalent carbon content of 0.09% shows a continuous increase, which results in a maximum at the end of testing. In the case of the type B steel grades, F_C increases quickly and reaches a plateau, where the contraction force remains nearly constant. Steel 5 has

a similar characteristic as the steels grades B, but shows a decrease after reaching a maximum, which potentially results from crack formation.

Calculation Results

Figure 3 shows the calculated accumulated strain along the solidified steel shell at the end of testing for each steel type. The shell thickness is replaced by the temperature distribution from T_{surf} to ZST. Therefore, the existing phase distribution of the solidified steel shell at the end of the experiment can be illustrated. A comparison of the three different steel grades clearly shows the influence of the existing phases on the development of the thermal strain inside the steel shell.

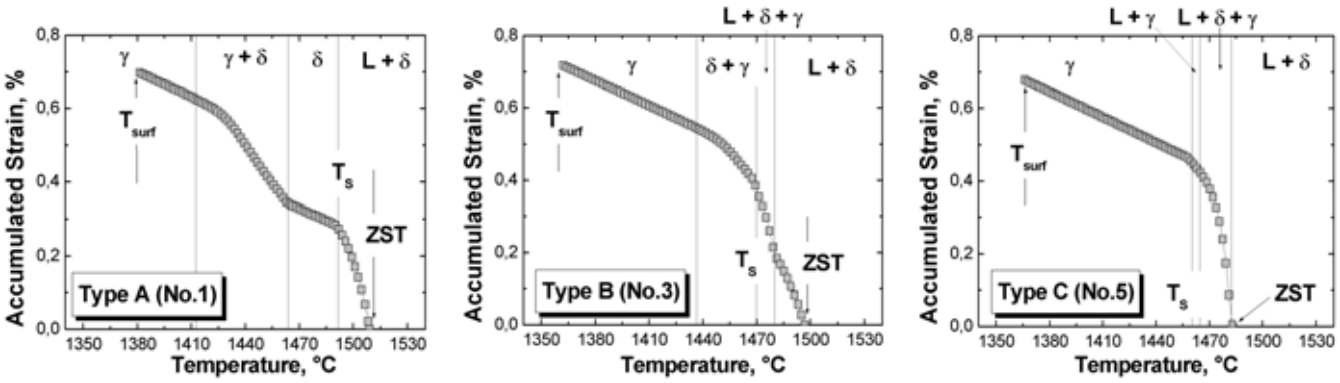

Figure 3: Calculated accumulated strain of different steel grades along the solidified steel shell

The different phase transformation sequences of type A, B and C steel grades and the resulting phase distribution inside the solidifying steel shell lead basically to a different development of the contraction during initial solidification. The type B steel grades reach the maximum F_C within a few seconds of solidification.

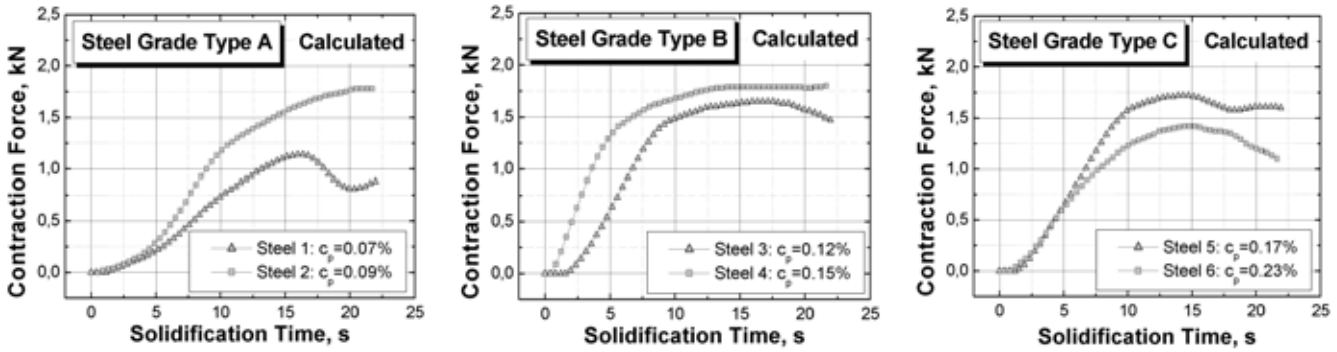

Figure 4: Calculated contraction force of the tested steel grades as a function of solidification time

Figure 4 shows the calculation results using the above thermo-mechanical model considering hardening and softening mechanisms. A comparison of the experimentally determined contraction forces with the calculated curves shows an excellent agreement. In the model, the material constants C and m (see Table II) taken from the equation of the temperature-dependent parameter K_P were utilized as fitting

parameters. It should be noted that the illustrated calculation results are strongly influenced by the softening term in the modeling procedure and therefore by the plastic relaxation rate. The calculations have shown that the plastic relaxation rate increases nearly linearly with time and depends on the carbon content. With increasing carbon content the plastic relaxation rate tends to increase. This behavior agrees with the prediction of Wray [18], who reported a reduction in work hardening with increasing carbon content, which in part corresponds to an increase in the rate of softening.

Example of an Application

Uneven shell formation as a function of the carbon content was first pointed out by Singh and Blazek [19] using systematic pilot investigations. Generally, shell deformation due to thermal contraction is assumed to depend on the balance between shell strength and the bending moment acting on the shell due to ferrostatic pressure [20]. Suzuki et al. [21] calculated the deflection of the solidifying shell assuming that the shell was equivalent to a beam and pointed out that peritectic medium carbon steels have a higher strength and larger contraction than low carbon steels just below T_S. Therefore, the shell deflection of peritectic medium carbon steels is not straightened by the ferrostatic pressure.

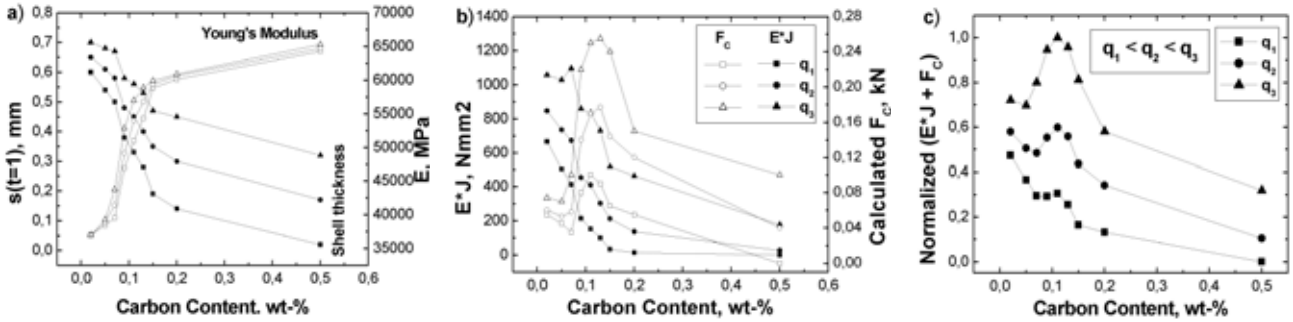

Figure 5: Shell thickness, Young's modulus a), bending strength, the calculated contraction force b) and the normalized ($E \cdot J + F_C$) curve c) as a function of carbon content for three different heat fluxes q

Therefore, it is reasonable to take the generated force due to the contraction into consideration. From static casting experiments [22] and from investigations of breakout shells [23, 24] it appears that an appreciable shell contraction occurs approximately at Z = 25 mm below the meniscus. Assuming a typical casting speed of 1.5 m/min one obtains a solidification time t of 1.0 s. Figure 5a shows the results of the calculated shell thickness s and the Young's modulus E as a function of the carbon content using three different heat fluxes ($q_1 < q_2 < q_3$) and a constant super heat at the time t = 1s. E is determined assuming an average shell temperature $(T_{surf}+T_S)/2$ and the simple mixture rule to consider the Fe-phase. As expected, both s and E increase with increasing heat flux. With rising carbon content s decreases and E increases due to the increasing amount of γ-Fe. The strength of the shell can be expressed using the bending strength, which is the product of the Young' modulus E and the inertia momentum J. Following the model proposed by Wolf and Kurz [20], the bending strength can be calculated using $J = (dZ \cdot s^3)/12$ (dZ=1). Figure 5b shows the results of these calculations together with the determined F_C using the model described above!). Although E increases with carbon content, the bending strength decreases with increasing carbon content, due to the strong influence of the shell thickness in the equation of J. The calculated F_C shows a maximum between a carbon content of 0.1 wt-% and 0.16 wt-% for all three heat fluxes, which is in line with the experiment.

Assuming that the bending strength as well as the contraction force act against the ferrostatic pressure, Figure 5c shows the summation curve ($E \cdot J + F_C$) of these two parameters., where the values are normalized between 0 and 1. In consideration of the assumed conditions (Z=25 mm) the ferrostatic pressure is independent of the carbon content and the heat flux. It should be mentioned that the curves in Figure 5c have to be understood as a tendency for depression formation (uneven shell growth). Therefore, it can be seen that with increasing heat flux the tendency towards depression formation increases, where the maximum forms between a carbon content of 0.1 wt-% and 0.16 with increasing heat flux.

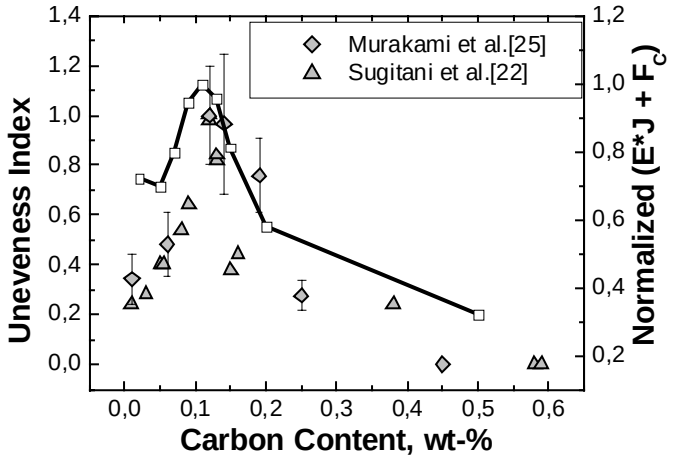

Figure 6: Uneven shell growth (uneven index) as a function of carbon content together with the normalized ($E \cdot J + F_C$) curve for q_3

Figure 6 shows two examples of the effect of the carbon content on the uneven shell growth derived by Sugitani and Nakamura [22] and Murakami et al.[25] from laboratory tests, where the illustrated values are normalized assuming an "unevenness index" between 0 and 1. In addition, the summation curve ($E \cdot J + F_C$) for heat flux q_3 is illustrated in the figure. It can clearly be seen that the characteristic is very similar to the experimentally determined uneven shell growth as a function of temperature.

Conclusion

The SSCT test is a proven method for the characterization of high-temperature mechanical properties and the crack susceptibility of steel under continuous casting conditions. The current paper presents an enhancement of this experiment in order to measure the contraction force during initial solidification of different steel grades. The experimentally determined results of these measurements are illustrated and discussed. Furthermore, a thermo-mechanical model of the contraction force test was developed. The model is based on the simplified geometry of the solidifying cross-section using an elasto-plastic approach. The necessary material parameters for the thermal, elastic and plastic strain are summarized and discussed. In addition, the results of the calculations are presented. Considering hardening and softening mechanisms, the calculated curves are in very good agreement with the experiment.

Finally, the importance of the contraction force concerning the uneven shell growth during initial solidification in the continuous casting process is demonstrated. Both the contraction force and the bending strength were taken into account in order to show the tendency of depression formation.

References

1. M. M. Wolf, "Initial Solidification and Strand Surface Quality of Peritectic Steels," *Continuous Casting, Volume Nine*, (Iron and Steel Society/AIME, 410 Commonwealth Drive, Warrendale, PA 15086-7528, USA, 1997)
2. H. Hiebler and C. Bernhard, "Mechanical properties and crack susceptibility of steel during solidification," *Steel Research*, 69 (8+9) (1999), 349-355.
3. C. Bernhard, H. Hiebler and M. Wolf, "Simulation of shell strength properties by the SSCT test," *ISIJ International*, 36 (Supplement) (1996), 163-166.
4. C. Bernhard, H. Hiebler and M. Wolf, "How fast can we cast?" *Ironmaking and Steelmaking*, 27 (6) (2000), 450-454.
5. A. A. Howe, „Segregation and Phase Distribution during Solidification of Carbon, Alloy and Stainless Steel," *EUR 13303*, (ECSC, Luxembourg, 1991)
6. R. Pierer, C. Bernhard and C. Chimani, "Experimental and analytical analysis of high-temperature mechanical properties of steel under continuous casting conditions" (Paper presented at the 12th International Conference on Computational Methods and Experimental Measurement, Malta, 20 – 22 June 2005), 757-768.
7. R. Pierer, C. Bernhard and C. Chimani, "Evaluation of Common Constitutive Equations for Solidifying Steel," *BHM*, 150 (2005), 163-169.
8. K. Hartse, "Untersuchungen zur Schrumpfung und zur Entstehung von mechanischen Spannungen während der Erstarrung und nachfolgender Abkühlung zylindrischer Blöcke aus Fe-C-Legierungen" (Ph.D thesis, TU-Clausthal, 1989)
9. I. Jimbo and A. A. W. Cramb, "The Density of Liquid Iron--Carbon Alloys," *Metallurgical Transactions B*, 24 (1993), 5-10.
10 M. Uehara, I. V. Samarasekera and J. K. Brimacombe, "Mathematical Modelling of Unbending of Continuously Cast Steel Slabs," *Ironmaking and Steelmaking*, 3 (3) (1986), 138-153.
11. K. Harste and K. Schwerdtfeger, "Thermomechanical properties of iron: viscoplasticity of ferrite and of austenite-ferrite mixtures," *Materials Science and Technology*, 12 (5) (1996), 378-384.
12. K. Harste, T. Suzuki and K. Schwerdtfeger, "Thermomechanical properties of steel: viscoplasticity of gamma iron and gamma Fe-C alloys," *Materials Science and Technology*, 8 (1) (1992), 23-33.
13. Bernhard Ilschner, *Hochtemperatur-Plastizität* (Berlin, Heidelberg, New York: Springer-Verlag, 1974)
14. M. Verdier, Y. Brechet and P. Guyot, "Recovery of AlMg alloys: flow stress and strain-hardening properties," *Acta Materialia*, 47 (1) (1999), 127-134.
15. A. Smith, H. Luo, D. N. Hanlon, J. Sietsma, and S. Van Der Zwaag, "Recovery Processes in the Ferrite Phase in C-Mn Steel," *ISIJ International*, 44 (7) (2004), 1188-1194.

16. C. Bernhard and G. Xia, “Influence of alloying elements on thermal contraction of peritectic steels during initial solidification,” *Ironmaking and Steelmaking*, 33 (2006) 52-55.

17. C. Bernhard, , G. Xia, “Influence of alloying elements on thermal contraction of peritectic steels during initial solidification,” (Paper presented at the 4th European Continuous Casting Conference, Birmingham, UK , 14-16 October 2002), 131-138.

18. P. J. Wray, “Effect of Carbon Content on the Plastic Flow of Plain Carbon Steels at Elevated Temperatures,” *Metallurgical Transactions A*, 13 (1982), 125-134.

19. S. N. Singh and K. E. Blazek, “Heat Transfer and Skin Formation in a Continuous-Casting Mold as a Function of Steel C Content,” *Journal of Metalls*, 26 (10) (1974), 17-27.

20. M. M. Wolf and W. Kurz, “The Effect of Carbon Content on Solidification of Steel in the Continuous Casting Mold,” *Metallurgical Transactions B*, 12 (1) (1981) 85-93.

21. M. Suzuki, C. H. Yu, H. Sato, Y. Tsui, H. Shibata and T. Emi, “Origin of heat transfer anomaly and solidifying shell deformation of peritectic steels in continuous casting,” *ISIJ International*, 36 (Supplement) (1996), 171-174.

22. Y. Sugitani and M. Nakamura, “Influence of Alloying Elements on Non-Uniform Solidification in Continuous Casting Moulds,” *Tetsu-to-Hagane*, 65 (1979), 1702-1711.

23. M. M. Wolf, and W. Kurz, “Solidification of Steel in Continuous-Casting Moulds,” (Paper presented at Solidification and Casting of Metals England, July 1979), 287-294.

24. H. Frederiksson and M. Thegerström, *Scandinavian Journal of Metallurgy*, 8 (1979) 323-240.

25. H. Murakami, M. Suzuki, T. Kitagawa and S. Miyahara, “Control of Uneven Solidified Shell Formation of Hypo-Peritectic Carbon Steels in Continuous Casting Mold,” *Tetsu-to-Hagane*, 78 (1992) 105-11.